(For presentation at the Gas Bearing Symposium, sponsored by ONR, Washington, D.C., Oct. 1959)

EXPERIMENTS WITH ROTATING, 10-INCH DIAMETER EXTERNALLY PRESSURIZED AIR THRUST BEARINGS

By Zolton N. Nemeth and William J. Anderson

Lewis Research Center
National Aeronautics and Space Administration
Cleveland, Ohio

ABSTRACT

Experimental studies were made with three parallel surface capillary compensated bearings at normal temperatures. Stationary plates contained four sector shaped recesses. Ratios of recess radius to plate radius of 1/3 and 2/3 were investigated. Bearing airflows and plate clearances were measured at speeds to 14,500 rpm and loads to 4000 pounds. From measurements of bearing clearance close to the bearing axis, airflow, and pressure profile, it was deduced that the bearing plates dished possibly because of pressure forces and thermal gradients. It is shown analytically that plate dishing has a marked effect on the theoretical pressure profile, airflow, and load capacity.

INTRODUCTION

Conventional bearing and lubricant combinations (such as oil lubricated rolling contact or hydrodynamic bearings) are marginal for operation above 750° F and unsuitable for use in the 1000° to 1500° F region. Other bearing types and lubricants are required to operate satisfactorily at extreme temperatures. Certain gases, such as air, are known to be stable at these high temperatures and may be used as well as liquids in fluid dynamic bearings. The load capacity of hydrodynamic or self acting bearings lubricated with gases will be low because of the low viscosities of the gases. However, since the viscosity of gases increase with temperature, the load carrying capacity of a self-acting bearing would also increase with temperature. For higher load applications the load carrying capacity of the bearing can be built up by pressure supplied from some external source. This type of bearing is known as an externally pressurized bearing.

The object of this investigation was to study the performance of a large, heavily loaded rotating externally pressurized air thrust bearing at room temperature with no temperature gradients imposed from outside causes. Most experimental gas bearing work has been conducted with rather small bearings with resultant low load capacities although at very high rotative speeds. It was felt that experimental work with a larger bearing was needed because of the many applications such as gas turbine engines and stationary engines requiring bearings to support loads up to several tons. Results obtained

with small bearings cannot be extrapolated to larger bearing sizes with any degree of certainty because of gas dynamics considerations and because of other unknowns such as distortion and alinement problems. With large bearings a relatively low air pressure can be employed while still maintaining a high load capacity. This makes it possible to utilize the compressor output of a gas turbine engine.

APPARATUS

Bearing Rig

The bearing test rig used in this investigation was that used in reference 1 to test large ball bearings under combined radial and thrust load conditions. A detailed description of the bearing rig, drive equipment, lubrication systems, and temperature measurement are given in reference 1. The test rig was modified to the extent required to accept parts for the air thrust bearing and test shaft.

A schematic drawing of the modified rig and test bearing is shown in figure 1. The rotating test air bearing plate is cantilever mounted at the end of the shaft near a cylindrical roller bearing. The stationary test air bearing plate is supported by a self alining spherical roller bearing. Parallelism of the air bearing plate surface is thus maintained. The stationary test air bearing plate assembly is balanced by a counterweight (not shown in the figure). Thrust, or axial load, was applied by means of a flexible stainless-steel bellows which, when pressurized with oil, exerted a force against a floating drum that transmitted the thrust load (without friction) to the shaft through an angular contact ball bearing. The drum floated in an externally pressurized oil bearing. This method of load application introduced considerable damping into the system and minimized any chances of bearing instabilities developing.

The air supply was 125 psig service air. Solid particles and liquid water were removed from the air by a separator and a filter. No effort was made to dry the air. Airflow was measured by a precalibrated rotameter. The air pressure in the rotameter was kept at 100 psig to maintain constant air density in order to simplify the flow calibration. Manifold pressure at the inlet to the flow resistance tubes was set to the desired value by adjusting flow control valves.

Temperature Measurement

Six iron-constantan thermocouples were located in each stationary air-bearing plate as shown in figures 2(a) to (c). The thermocouples were embedded in the bearing plate and machined flush with the bearing surface so as not to disturb the airflow. Additional air temperatures were measured just outside the air bearing at the clearance between the two plates and in the air bearing housing behind the stationary air bearing plate. Temperatures could be read to an accuracy of $\pm 1^{\circ}$ F.

Pressure Measurement

Nine pressure taps were located in each stationary plate as shown in figures 2(a) to (c). Air pressures were also measured outside the air bearing at several points in the air supply line. Each pressure tap in the bearing was connected to a precalibrated pressure gage through 0.048 inch inside diameter tubing. Pressure could be read to an accuracy of ±1 psi.

Clearance Measurement

The test bearing clearance or gap was measured during operation in two ways: mechanically with a dial indicator (0.0001 inch per division) and electronically with a capacitance proximity meter. The dial indicator frame was attached rigidly to the nonrotating plate. It was actuated by a spring loaded rod held against a small pivot bearing in the rotating plate. It measured bearing clearance at the center of the bearing (fig. 1). The capacitance proximity meter measured the bearing clearance 1.19 inches from the center of the air bearing.

The dial indicator was used mainly to calibrate the electronic proximity gage but it was also used several times during running to check the readings of the capacitance proximity gage.

The capacitance proximity gage is temperature sensitive because of the change of the dielectric properties of air in the bearing gap with temperature and the moisture content. The calibration curve moves without a change of slope as the air temperature changes in the bearing gap at the gage. A correction must be applied to the readings depending on the temperature and moisture content. Clearance could be determined to within 0.0001 inches with the capacitance gage.

Test Bearings

Three stationary plates differing in pad geometry were used for this investigation. The rotating plate was a plane faced disk. Figure 2 illustrates the geometry of the three stationary plates. Plates I and III (figs. 2(a) and (c)) had outer recess radii equal to 2/3 of the plate radius while plate II (fig. 2(b)) had an outer recess radius equal to 1/3 of the plate radius. Figure 2(d) shows the simple recess bearing configuration which is used in appendixes B and C for analysis purposes. In all three plates the recesses were approximately 0.050 inch deep.

The stationary and rotating plates were made of 440-C stainless steel hardened to Rockwell C-51 to 58. The mating surfaces were ground flat to within 0.0001 inch with a surface roughness of less than 8 microinches rms. The total runout of the rotating plate face was held within 0.0003 inch for all tests except those in which it was purposely set out of square 0.0015 inch.

Plates I and III were fed via capillary tubes 0.116 inch inside diameter by $25\frac{1}{2}$ inches long, and plate II through tubes 0.089 inside diameter by $36\frac{1}{2}$ inches long.

PROCEDURE

Measurements of flow pressure, temperature, and film thickness were taken after equilibrium temperature, pressure, and mass flow had been accomplished. Tests were run by first setting a speed and then obtaining equilibrium conditions for that speed. Data were then taken at the various bearing loads and manifold pressures desired.

The capacitance gage was calibrated at zero speed and at temperatures from room temperature to the maximum operating temperature (approximately 180° F) of the air bearing. The gages were zeroed with the bearing plates in contact under load. The zero reading at temperature was obtained by running the rig until the air bearing heated up and then quickly shutting down the rig and bringing the plates together. The rig was run over a speed range to obtain the various air bearing temperatures for calibration. The dial indicator calibration was constant over the temperature range (indicating negligible differential expansion) but the capacitance gage calibration changed because of the change in the dielectric constant of the air film. It was possible to obtain a curve giving the change of the capacitance gage calibration with temperature. The actual film thickness was then determined as a function of the proximity meter reading and the temperature.

The dial indicator measured the air film thickness at the center of the bearing and the capacitance gage at 1.19 inches from the center of the bearing so that dishing of the bearing plates (which was found later) could not be measured.

RESULTS AND DISCUSSION

The results discussed herein are preliminary in nature and much remains to be learned about the operating characteristics and dependability of externally pressurized gas bearings subjected to conditions arising in actual applications. Unexpected phenomena were encountered and because of the incompleteness of the instrumentation, especially in regard to film thickness measurement, some of these phenomena can be explained qualitatively only.

One important general observation that is worth noting is the fact that no operating difficulties were encountered at any time. All of the test bearings operated without rubbing for several hundred hours. This investigation was not intended to uncover any instability characteristics but merely to explore in a preliminary way the operating characteristics of this type of bearing. As previously pointed out, the method of loading introduces considerable damping in the system so that instabilities would not be likely to appear.

Bearing Load

Figures 3 and 4 show the effect for plates I and II of bearing load on airflow, recess pressure and film thickness for no rotation and 7500 rpm, respectively. The expected trends in these variables are evident for both plate I ($r_r/r_a = 2/3$, figs. 3(a) and 4(a)) and for plate II ($r_r/r_a = 1/3$, figs. 3(b) and 4(b)). The airflow decreases with load because of the reduced film thickness. The film thickness must decrease to allow the recess pressure to increase until the external load can be supported.

The relation between film thickness and airflow warrants closer examination because the expected cubic relation ($G \sim h^3$) was not obtained. Since flow has been observed to vary with the cube of the clearance by a number of different experimenters (refs. 2 and 4), it was obvious that the measured film thickness was not that which was controlling the airflow. As noted previously the capacitance probe measured the clearance at 1.19 inches from the bearing axis, whereas the clearance of real importance as regards airflow was the mean effective clearance between the recess radius and the bearing outer radius. For example, in Fig. 3(a) the measured airflow and film thickness at loads of 1500 and 4000 lbs were, respectively, 200 lb/hr and 0.0046 inches and 165 lb/hr and 0.0022 inches. If the bearing plates had remained parallel, the reduction in airflow due to an increase in load from 1500 to 4000 pounds would have been far greater than that measured. These data, therefore, imply that distortion of the bearing plates took place. The data of Fig. 3 were obtained at no rotation with all the bearing parts at essentially constant temperature so that thermal distortions are improbable. Therefore, it is possible that the bearing faces were distorted from plane surfaces to convex surfaces by gas pressure; the bearing clearances outside the recesses were greater than those measured by the capacitance probe, the discrepancy increasing with load. Accurate calculations of plate deflections would be very difficult to make because of the complex shape of the bearing plates and because of uncertainties in the rigidity of the plate support.

For purposes of checking the feasibility of this reasoning, deflections were calculated for a uniformly loaded circular plate resembling the rotating plate. These were found to be 0.0011 inches at 1500 pounds load and 0.0031 inches at 4000 pounds load. Assuming these deflections (which is improbable) the perimeter clearances would then be 0.0057 inches (0.0046 + 0.0011) and 0.0053 inches (0.0022 + 0.0031). The expected flow ratio would then be $(0.0057/0.0053)^3$ or 1.25. The measured flow ratio was 200/165 or 1.21. This approximation is admittedly crude but it serves to illustrate the feasibility of the argument.

Similar conclusions may be deduced from the data of Fig. 4 although here another variable, thermal distortion of the bearing plates, enters the picture. This will be discussed more completely later on.

Bearing Speed

The effect of bearing speed on bearing airflow is shown in Fig. 5. For most of the tests the airflow remained fairly constant with speed. This would indicate a fairly constant effective film thickness because the effect of rotation on airflow is minor for the range of speeds covered in these experiments. Expressions for mass flow with inertia effects taken account of are derived in appendix B and in Ref. 3. The symbols used in appendixes B and C are defined in appendix A. The work in appendix B was completed some time before the publication of Ref. 3, but is included here as background material for appendix C. Figure 6 shows the results of some calculations for the simple bearing configuration shown in Fig. 2(d). For a constant h, the theoretical variation in G over the speed range of this investigation is very small. With the constancy of mass flow over the range of operating speeds, one would then expect little change in the measured bearing film thickness. However, this was not the case. Figure 7 shows typical data obtained with plates I and III ($r_r/r_a = 2/3$) at 3 loads and Fig. 8 shows similar data for plate II ($r_r/r_a = 1/3$). In every test, the film thickness (measured close to the bearing axis) increased substantially with speed. In many tests, clearance measurements obtained with the capacitance probe were checked with the dial indicator system and found to be correct. The relations of appendix B were used, together with the experimentally measured airflows and recess pressures, to calculate the effective clearance at each test condition. The effective clearance is defined as that constant clearance which would result in an airflow equal to the measured airflow at the measured recess pressure. These calculated effective clearances are plotted on Figs. 7 and 8. They are nearly constant with speed and show an increasing disparity with the measured clearances as the speed was increased.

Bearing and Air Temperatures

The temperature patterns which existed within the test bearing were sharply influenced by the behavior of the adjacent cylindrical roller bearing. Figure 9 shows some temperature data of interest obtained from one test of plate II ($r_r/r_a = 1/3$). Both the air bearing temperature (as measured by thermocouple A, fig. 2(b)) and the air-out temperature increase linearly with speed. At speeds above 9000 rpm the air-out temperature exceeds the roller bearing temperature indicating that considerable heat is generated within the air film.

Figure 10 shows temperature profiles for both ratios of recess radius. At the higher speeds significant temperature rises occur in the bearing plate at radii greater than the recess radius. Heating effects are much more apparent in the 1/3 recess radius ratio bearing (fig. 10(b)) than in the 2/3 recess radius ratio bearing (fig. 10(a)). This is because of the much greater area of thin film (and consequent high shear rate) in the bearing with the small recesses.

Plate Dishing

From the mass flow and clearance data it was concluded that the rotating bearing plate was dishing as the speed was increased. Heat flow into the

rotating plate from the adjacent cylindrical roller bearing produced the axial temperature gradient across the rotating plate which caused it to dish.

The effects of plate dishing were most apparent with the 1/3 radius ratio plate (plate II, fig. 2(b)). A marked change in pressure profile and in the recess pressure at constant load was noted with increasing speed. Recess pressures at various bearing speeds at 3000 pounds load for plate II are shown in Fig. 11. Figure 12 shows pressure profile data for plate II measured on the lands between the recesses. Note that the pressure profiles extend well inside the recess radius before the pressures reach the recess pressure.

To help explain these data, an extension of the analysis of appendix B was made to include the effects of plate dishing such as shown schematically (fig. 13). Since the effects of rotation were negligible within the speed range investigated, speed was neglected as a first approximation. The analysis of plate dishing effects for the nonrotating case is given in appendix C. Some of the calculations based on this analysis are given in Figs. 13, 14, 15, and 16. It is seen that the dishing parameter ξ has a strong effect on the load capacity and the airflow. ξ is defined as the ratio of the amount of dishing (Δh) to the minimum clearance h_m. Figures 13 and 14 indicate that both airflow and load capacity increase as ξ increases. These effects were found to be stronger for the 1/3 recess radius ratio than for the 2/3 ratio.

From Fig. 14 the recess pressure required to support a given load with various degrees of dishing (values of ξ) can be determined. These data are shown in Fig. 15.

Pressure profile data from the analysis of appendix C are shown in Fig. 16 for a recess radius ratio of 1/3 and a recess pressure of 94.7 psia. Similar data were plotted for other recess pressures so that analytical curves similar to the experimental data of Fig. 12 could be plotted. The experimentally measured values of recess pressure at each speed were used to derive values of ξ necessary to support the load. Pressure profiles for each of these p_r's and ξ's are shown in Fig. 17. The marked similarity between the theoretical pressure profiles of Fig. 17 and the experimental pressure profiles of Fig. 12 is apparent.

In addition to the pressure profile data, the measured air bearing plate and roller bearing temperatures seem to support the hypothesis that the air bearing plate dished. Although Figs. 9 and 10(b) indicate that both the maximum roller bearing temperature and the plate temperature reached about 220° F it is important to note that the bulk of the heat flow from the roller bearing to the bearing plate (see fig. 1) took place within a radius of 2.5 inches from the bearing center. At this radius the maximum plate temperature was 190°. Calculations show that, for an unrestrained plate resembling the rotating plate, an axial temperature gradient will produce a dish of approximately 0.0002 inches per degree F of gradient.

The actual shape of the bearing plates during test is undoubtedly very complex, resulting from a composite of pressure forces and temperature gradients.

These analyses are included only in an attempt to explain qualitatively the experimental results.

Plate Misalinement

In order to further investigate the effects of geometric inaccuracies on bearing performance, the rotating face was set 0.0015 inch out of square. All previous tests had been run with the total runout of the rotating face held within 0.0003 inch. Plate I (fig. 2(a)) was used for these tests. Bearing airflow and film thickness were relatively unaffected by the out of square condition.

Cyclic fluctuations in pressure, promoted by fluctuations in film thickness, were noted but bearing performance was otherwise normal. In general this out of square condition emphasized again the relative insensitivity of this type of gas bearing to distortion and geometrical inaccuracies.

SUMMARY OF RESULTS

Experiments were conducted with three parallel surface, capillary compensated, rotating 10 inch diameter externally pressurized air thrust bearings at normal temperatures. Stationary plates contained four sector shaped recesses with ratios of recess radius to bearing radius of 1/3 and 2/3. Bearing airflows and plate clearances were measured at speeds to 14,500 rpm and loads to 4000 pounds. The following results were obtained:

1. Bearing operation was, in every instance, completely satisfactory and no damaging face rubbing occurred at any time. As an example of required airflows, a load of 3000 pounds could be supported with an airflow of 67 pounds per hour.

2. From measurements of bearing clearance close to the bearing axis, airflow and pressure profile, it was deduced that the bearing plates dished because of pressure forces and thermal gradients. Thermal distortion had a significant effect on bearing pressure profile. An analysis is presented which takes into account the effect of plate dishing on airflow, pressure profile and load capacity. The experimental results correlate qualitatively with the analysis.

3. Airflow was relatively unaffected by speed.

4. At low speeds, bearing temperatures were fairly constant but at higher speeds the air incurred significant temperature rises. Air temperature rise was greatest in the bearing with the smallest area recesses because of the greater area of thin film and, consequently, high shear rate.

5. Bearing operation was relatively insensitive to geometric inaccuracies as evidenced by the minor effect of plate dishing, and by the fact that an out of square condition of 0.0015 inch of the rotating face had little effect on bearing operating characteristics.

APPENDIX A

SYMBOLS

G	weight flow, lb/hr
h	film thickness, in.
h'	$h - h_m$, in.
Δh	depth of plate dish, in.
K_1	$3/10(\omega^2/RT)$
K_2	$6\mu GRT/\pi h^3$
K_3	$6\mu GRT/\pi h_m^3$
p	pressure, psia
R	gas constant, in. lb/lb $^{\circ}F$
r	radius, in.
r	radial coordinate
T	temperature, $^{\circ}F$ abs
u	radial velocity, in./sec
v	tangential velocity, in./sec
W	load, lb
z	coordinate normal to bearing surface
θ	r^2, a dummy variable
λ	radius of curvature of the dished surface, in.
μ	viscosity, lb sec/sq in.
ξ	dishing parameter, $\Delta h/h_m$, dimensionless
ρ	density, lb/cu in.
ω	angular velocity, rad/sec

Subscripts:

a outside or atmospheric

e effective

m minimum or manifold

r recess

APPENDIX B

EFFECT OF INERTIA FORCES ON MASS FLOW AND LOAD CAPACITY

Although the following analysis appears in somewhat the same form in Ref. 3, it was completed before the publication of Ref. 3 and is included here for the convenience of the reader as background material for appendix C. Consider the simple single recess bearing of Fig. 2(d).

The equation for the radial pressure gradient is

$$\frac{\partial p}{\partial r} = \mu \frac{\partial^2 u}{\partial z^2} + \frac{v^2}{r} \tag{B1}$$

Assuming a linear variation in tangential velocity across the clearance

$$v = \frac{\omega r z}{h} \tag{B2}$$

With assumption (B2), using the perfect gas law and assuming isothermal flow, Eq. (B1) can be integrated to give

$$p^2 = e^{K_1 r^2}\left[p_a^2 e^{-K_1 r_a^2} + K_2 \int_{r^2}^{r_a^2} \frac{e^{-K_1\theta}}{\theta}\, d\theta\right] \tag{B3}$$

where θ is a dummy variable,

$$K_1 = \frac{3}{10}\frac{\omega^2}{RT} \tag{B4}$$

and

$$K_2 = \frac{6\mu G R T_a}{\pi h^3} \tag{B5}$$

where G, the weight flow, is defined as

$$G = 2\pi r \rho \int_0^h u\, dz \tag{B6}$$

$$p_r^2 = e^{K_1 r_r^2}\left[p_a^2 e^{-K_1 r_a^2} + K_2 \int_{r_r^2}^{r_a^2} \frac{e^{-K_1\theta}}{\theta}\, d\theta\right] \tag{B7}$$

The integral can be evaluated using the relation

$$\int \frac{e^{-K_1\theta}}{\theta}\, d\theta = \ln \theta + (-K_1\theta) + \frac{(-K_1\theta)^2}{2 \cdot 2!} + \frac{(-K_1\theta)^3}{3 \cdot 3!} + \cdots \tag{B8}$$

then

$$\int_{r_r^2}^{r_a^2} \frac{e^{-K_1\theta}}{\theta}\, d\theta = \left[\ln\left(\frac{r_a}{r_r}\right)^2 - K_1(r_a^2 - r_r^2) + \frac{K_1^2}{4}(r_a^4 - r_r^4) - \frac{K_1^3}{18}(r_a^6 - r_r^6) + \cdots\right] \tag{B9}$$

Equation (B8) is used to solve for the weight flow G with the recess pressure, p_r, the recess radius, r_r, the clearance, h, and the rotative speed, ω known. With G known Eq. (B3) can be used to solve for the pressure at any radius.

The load capacity is

$$W = \pi r_r^2(p_r - p_a) + 2\pi \int_{r_r}^{r_a} (p - p_a) r\, dr \tag{B10}$$

A digital computer was used to calculate G, p, and W with the first three terms of the series expansion in Eq. (B9) retained. As shown in Fig. 6 the effect of speed on weight flow G was very minor within the speed range of these experiments.

APPENDIX C

EFFECT OF PLATE DISTORTION ON MASS FLOW AND LOAD CAPACITY - NO ROTATION

Assume that the bearing plate distorts to a spherical shape, of radius λ

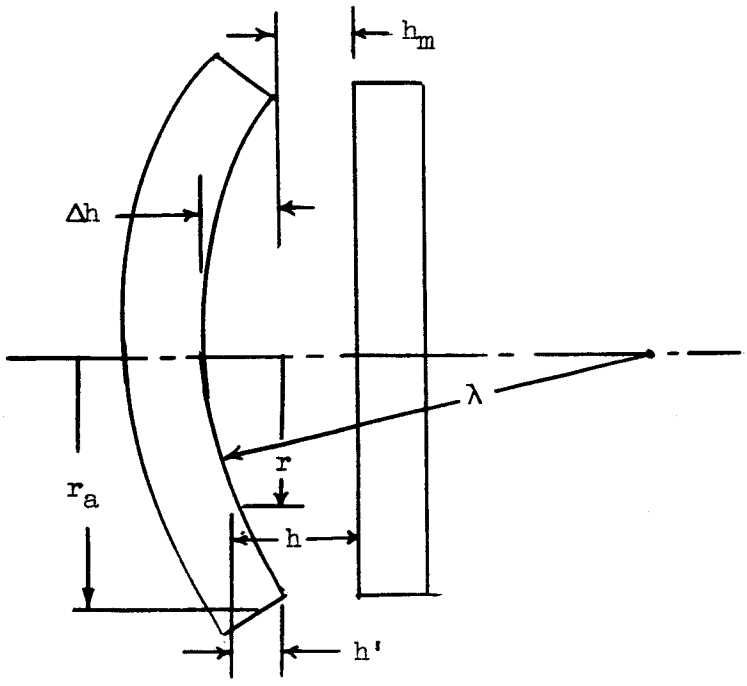

$$\lambda - (\Delta h - h') = \sqrt{\lambda^2 - r^2} \tag{C1}$$

$$(\lambda - \Delta h)^2 = \lambda^2 - r_a^2 \tag{C2}$$

From Eq. (C2), neglecting second orders of magnitude

$$\lambda = \frac{r_a^2}{2\Delta h} \tag{C3}$$

Likewise, from Eq. (C1)

$$2\lambda h' + r^2 - 2\lambda\Delta h = 0 \tag{C4}$$

$$h' = \frac{1}{2\lambda}\left(2\lambda\Delta h - r^2\right) \tag{C5}$$

Substituting (C3) into (C5)

$$h' = \Delta h\left[1 - \left(\frac{r}{r_a}\right)^2\right] \tag{C6}$$

From Eq. (B1) with $v = 0$

$$\frac{dp}{dr} = \mu \frac{\partial^2 u}{\partial z^2} \tag{C7}$$

u can be found by integrating Eq. (C7) twice, noting that $u = 0$ at $z = 0$ and $z = h$, or alternatively, by differentiating Eq. (B3). The following results

$$\frac{dp}{dr} = - \frac{6\mu GRT_a}{\pi} \left(\frac{1}{prh^3} \right) \tag{C8}$$

Since

$$h = h' + h_m \tag{C9}$$

$$\frac{dp}{dr} = - \frac{6\mu GRT_a}{\pi p} \frac{1}{(h' + h_m)^3 r} \tag{C10}$$

$$pdp = - \frac{6\mu GRT_a}{\pi} \frac{dr}{rh_m^3 \left\{ 1 + \frac{\Delta h}{h_m} \left[1 - \left(\frac{r}{r_a} \right)^2 \right] \right\}^3} \tag{C11}$$

Let

$$x = \frac{r}{r_a} \tag{C12}$$

$$dx = \frac{dr}{r_a} \tag{C13}$$

$$K_3 = \frac{6\mu GRT_a}{\pi h_m^3} \tag{C14}$$

$$\xi = \frac{\Delta h}{h_m} \tag{C15}$$

Then

$$pdp = \frac{-K_3 dx}{\left[1 + \xi(1 - x^2) \right]^3 x} \tag{C16}$$

Equation (C16) can be integrated to give

$$\frac{p^2 - p_r^2}{2} = -\frac{K_3}{\xi^3}\left[\frac{1}{4\left(\frac{1+\xi}{\xi}\right)\left[\left(\frac{1+\xi}{\xi}\right) - x^2\right]^2} + \frac{1}{2\left(\frac{1+\xi}{\xi}\right)^2\left[\left(\frac{1+\xi}{\xi}\right) - x^2\right]}\right.$$

$$\left. + \frac{1}{2\left(\frac{1+\xi}{\xi}\right)^3} \ln\left\{\frac{x^2/\xi}{\left(\frac{1+\xi}{\xi}\right) - x^2}\right\}\right]_{\frac{r_r}{r_a}}^{\frac{r}{r_a}} \qquad \text{(C17)}$$

$$p^2 = p_r^2 - \frac{2K_3}{\xi^3}\left(\frac{1}{\frac{4(1+\xi)}{\xi}\left[\frac{1+\xi}{\xi} - \left(\frac{r}{r_a}\right)^2\right]^2} - \frac{1}{\frac{4(1+\xi)}{\xi}\left[\left(\frac{1+\xi}{\xi}\right) - \left(\frac{r_r}{r_a}\right)^2\right]^2}\right.$$

$$+ \frac{1}{2\left(\frac{1+\xi}{\xi}\right)^2\left[\left(\frac{1+\xi}{\xi}\right) - \left(\frac{r}{r_a}\right)^2\right]} - \frac{1}{2\left(\frac{1+\xi}{\xi}\right)^2\left[\left(\frac{1+\xi}{\xi}\right) - \left(\frac{r_r}{r_a}\right)^2\right]}$$

$$\left. + \frac{1}{2\left(\frac{1+\xi}{\xi}\right)^3} \ln\left\{\left(\frac{r}{r_r}\right)^2 \frac{\left[\left(\frac{1+\xi}{\xi}\right) - \left(\frac{r_r}{r_a}\right)^2\right]}{\left[\left(\frac{1+\xi}{\xi}\right) - \left(\frac{r}{r_a}\right)^2\right]}\right\}\right) \qquad \text{(C18)}$$

Simplifying

$$p^2 = p_r^2 - 2K_3\left(\frac{1}{4(1+\xi)\left[1+\xi-\xi\left(\frac{r}{r_a}\right)^2\right]^2} - \frac{1}{4(1+\xi)\left[1+\xi-\xi\left(\frac{r_r}{r_a}\right)^2\right]^2}\right.$$

$$+ \frac{1}{2(1+\xi)^2\left[1+\xi-\xi\left(\frac{r}{r_a}\right)^2\right]} - \frac{1}{2(1+\xi)^2\left[1+\xi-\xi\left(\frac{r_r}{r_a}\right)^2\right]}$$

$$\left. + \frac{1}{2(1+\xi)^3} \ln\left\{\left(\frac{r}{r_r}\right)^2 \frac{\left[1+\xi-\xi\left(\frac{r_r}{r_a}\right)^2\right]}{\left[1+\xi-\xi\left(\frac{r}{r_a}\right)^2\right]}\right\}\right) \qquad \text{(C19)}$$

It can readily be seen that when $\xi = 0$, Eq. (C19) reduces to the equation for parallel plates and zero rotation.

The weight flow G is obtained from Eq. (C19) by substituting p_a for p and r_a for r.

$$G = \frac{2(p_r^2 - p_a)h_m^3}{12\mu R T_a} \times$$

$$\left[\frac{1}{\frac{1}{4(1+\xi)} - \frac{1}{4(1+\xi)\left[1+\xi-\xi\left(\frac{r_r}{r_a}\right)^2\right]^2} + \frac{1}{2(1+\xi)^2} - \frac{1}{2(1+\xi)^2\left[1+\xi-\xi\left(\frac{r_r}{r_a}\right)^2\right]} + \frac{1}{2(1+\xi)^3}\ln\left\{\left(\frac{r_a}{r_r}\right)^2\left[1+\xi-\xi\left(\frac{r_r}{r_a}\right)^2\right]\right\}} \right] \quad \text{(C20)}$$

The load capacity W is obtained by using pressure values from Eq. (C19)

$$W = \pi(p_r - p_a)r^2 + 2\pi\int_{r_r}^{r_a}(p - p_a)r\,dr \quad \text{(C21)}$$

REFERENCES

1. Anderson, W. J.: Performance of 110-Millimeter-Bore M-1 Tool Steel Ball Bearings at High Speeds, Loads, and Temperatures. NACA TN 3892, 1957

2. Pigott, Joseph D., and Macks, E. Fred: Air-Bearing Studies at Normal and Elevated Temperatures. Lubrication Engineering, vol. 10, no. 1, February, 1954.

3. Osterly, J. F., and Hughes, W. F.: The Effect of Lubricant Inertia in Hydrostatic Thrust Bearing Lubrication. Wear, vol. 1, no. 6, June 1958, pp. 465-471.

4. Licht, L., and Fuller, D. D.: A Preliminary Investigation of an Air-Lubricated Hydrostatic Thrust Bearing. ASME paper 54-LUB-18.

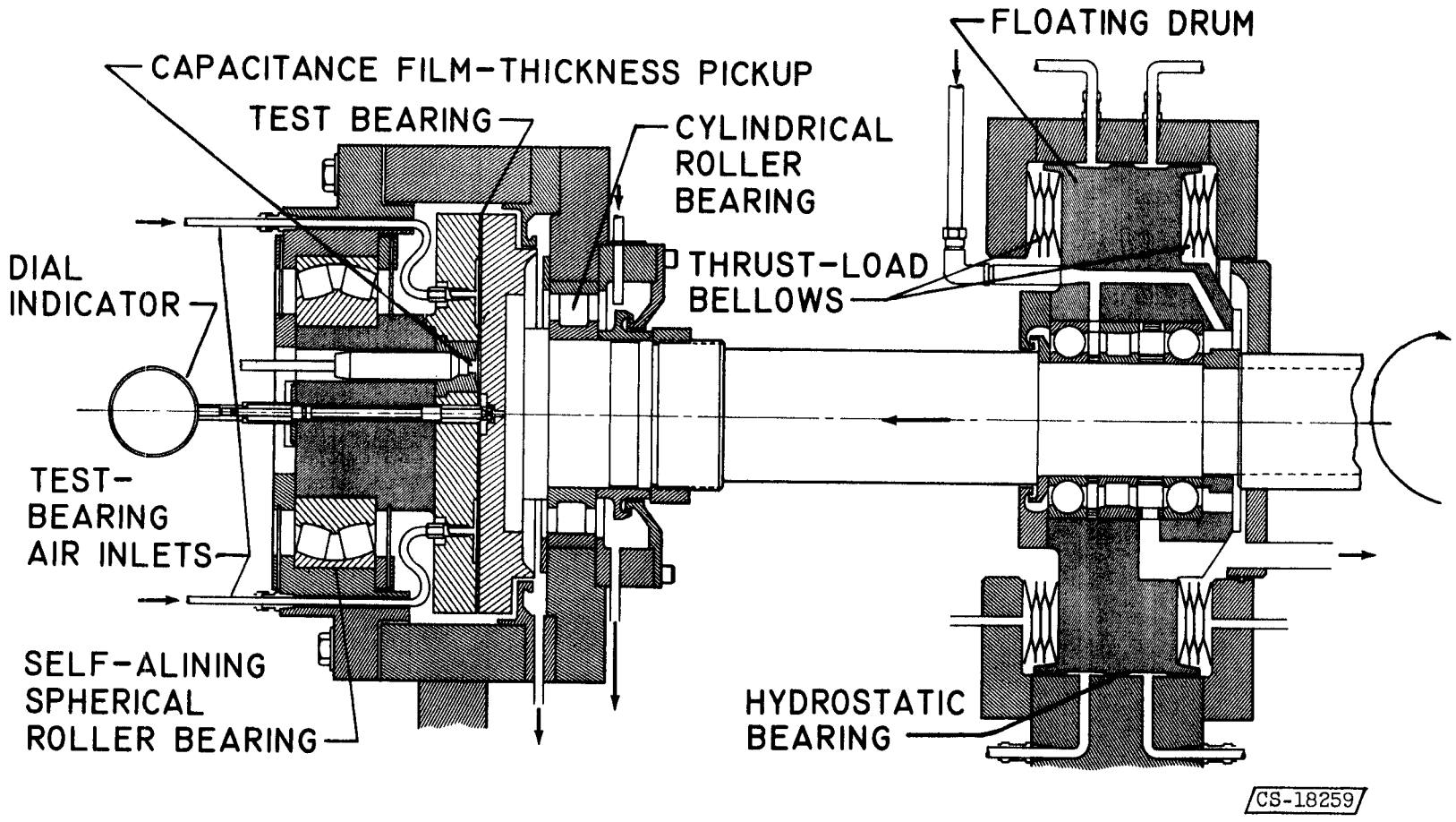

Fig. 1. - Schematic of air thrust bearing test rig.

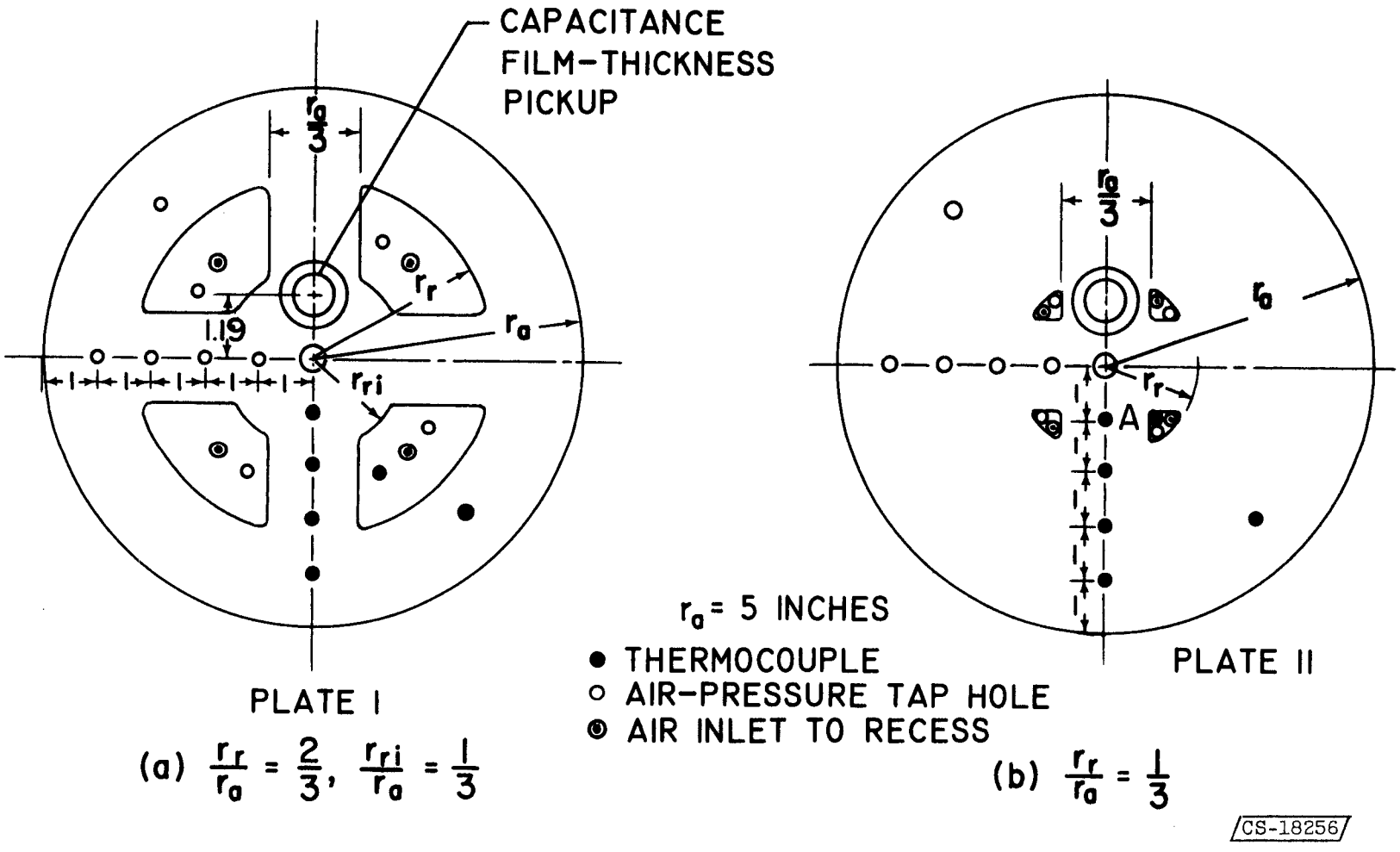

Fig. 2. - Externally pressurized air thrust bearing - stationary plates.

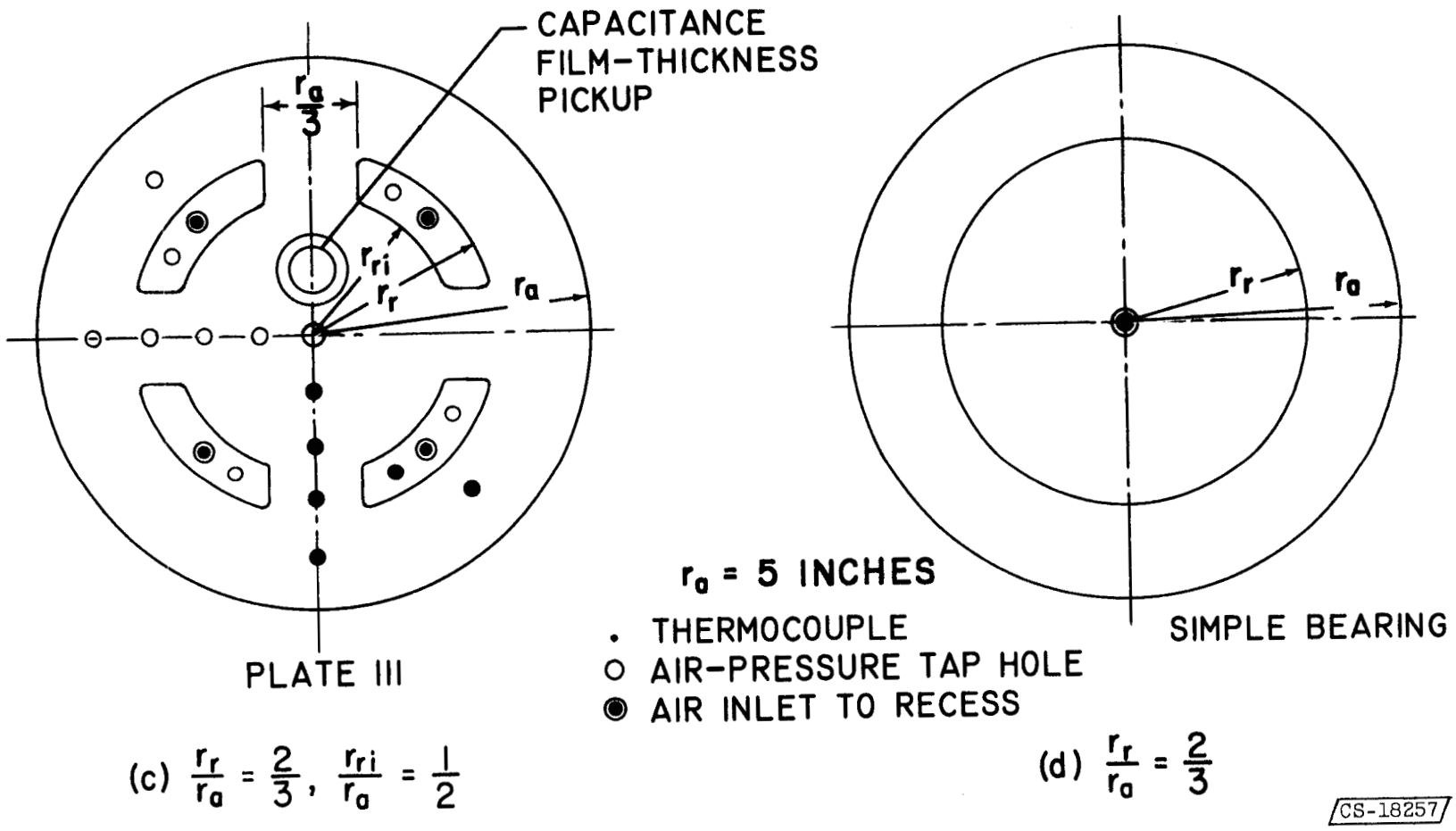

Fig. 2. - Concluded. Externally pressurized air thrust bearing-stationary plates.

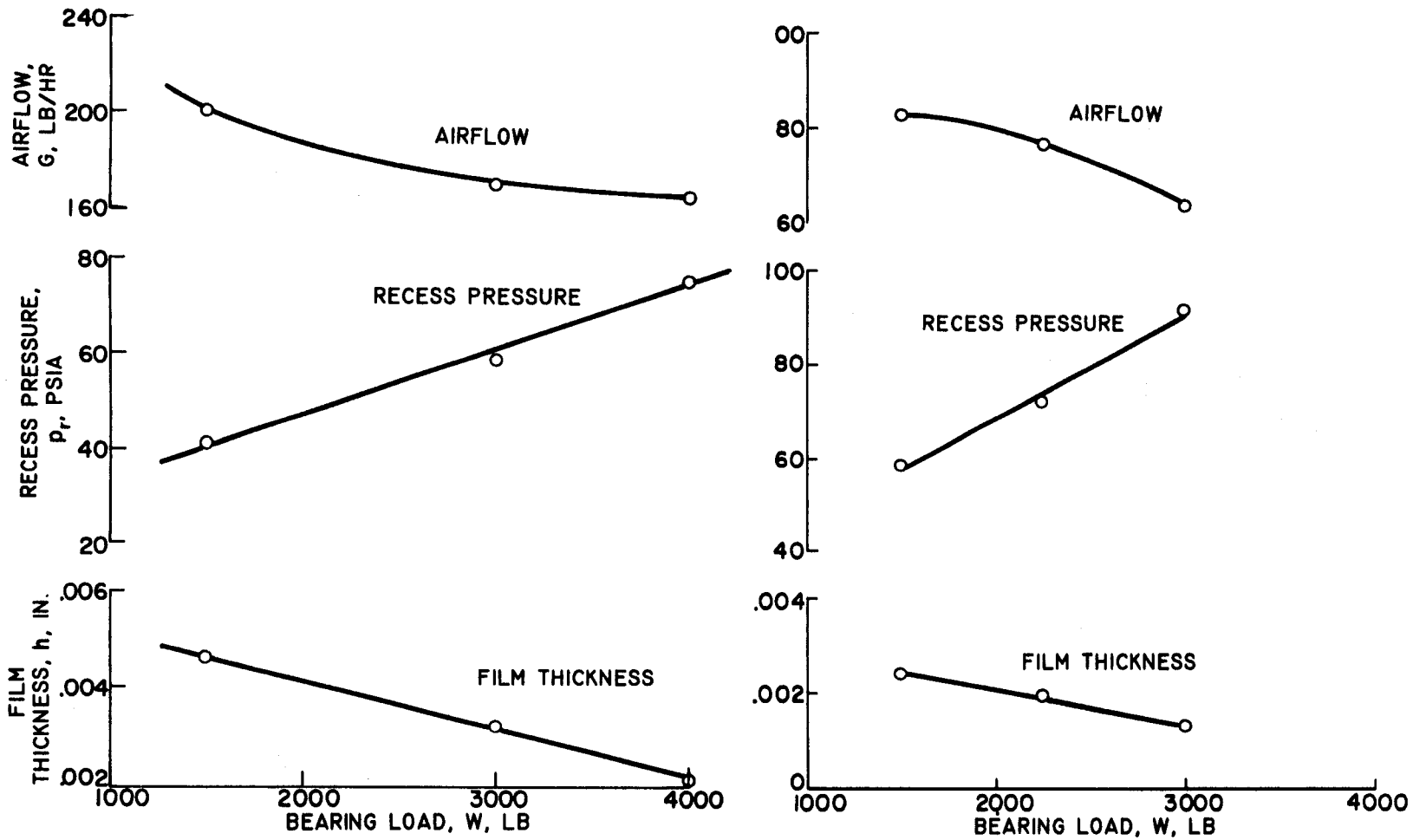

(a) r_r/r_a = 2/3, Plate I.

(b) r_r/r_a = 1/3, Plate II.

Fig. 3. - Effect of bearing load on airflow, recess pressure and film thickness. No rotation; p_m = 114.7 psia.

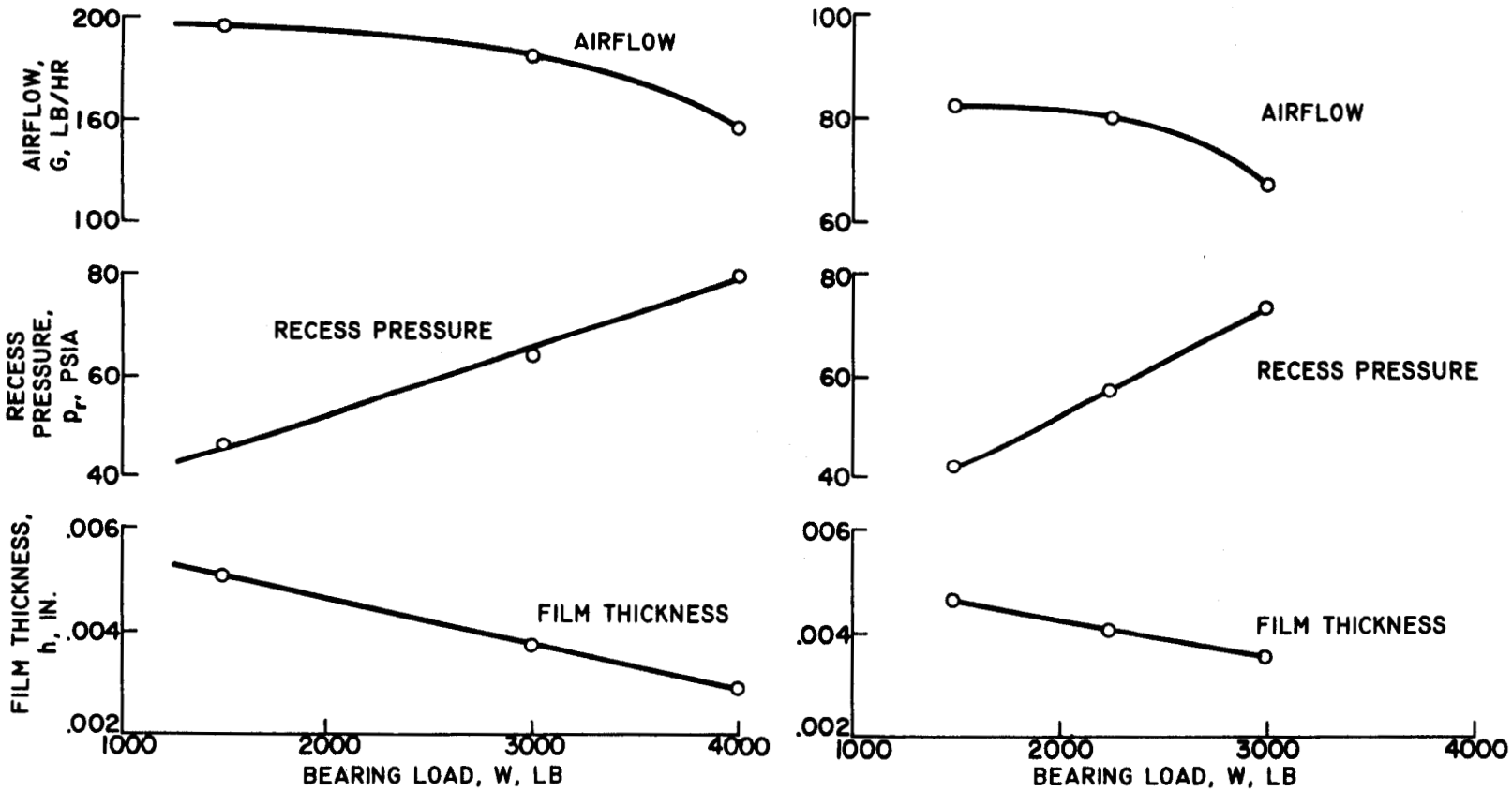

(a) r_r/r_a = 2/3, Plate I.

(b) r_r/r_a = 1/3, Plate II.

Fig. 4. - Effect of bearing load on airflow, recess pressure, and film thickness. Speed, 7500 rpm; p_m = 114.7 psia.

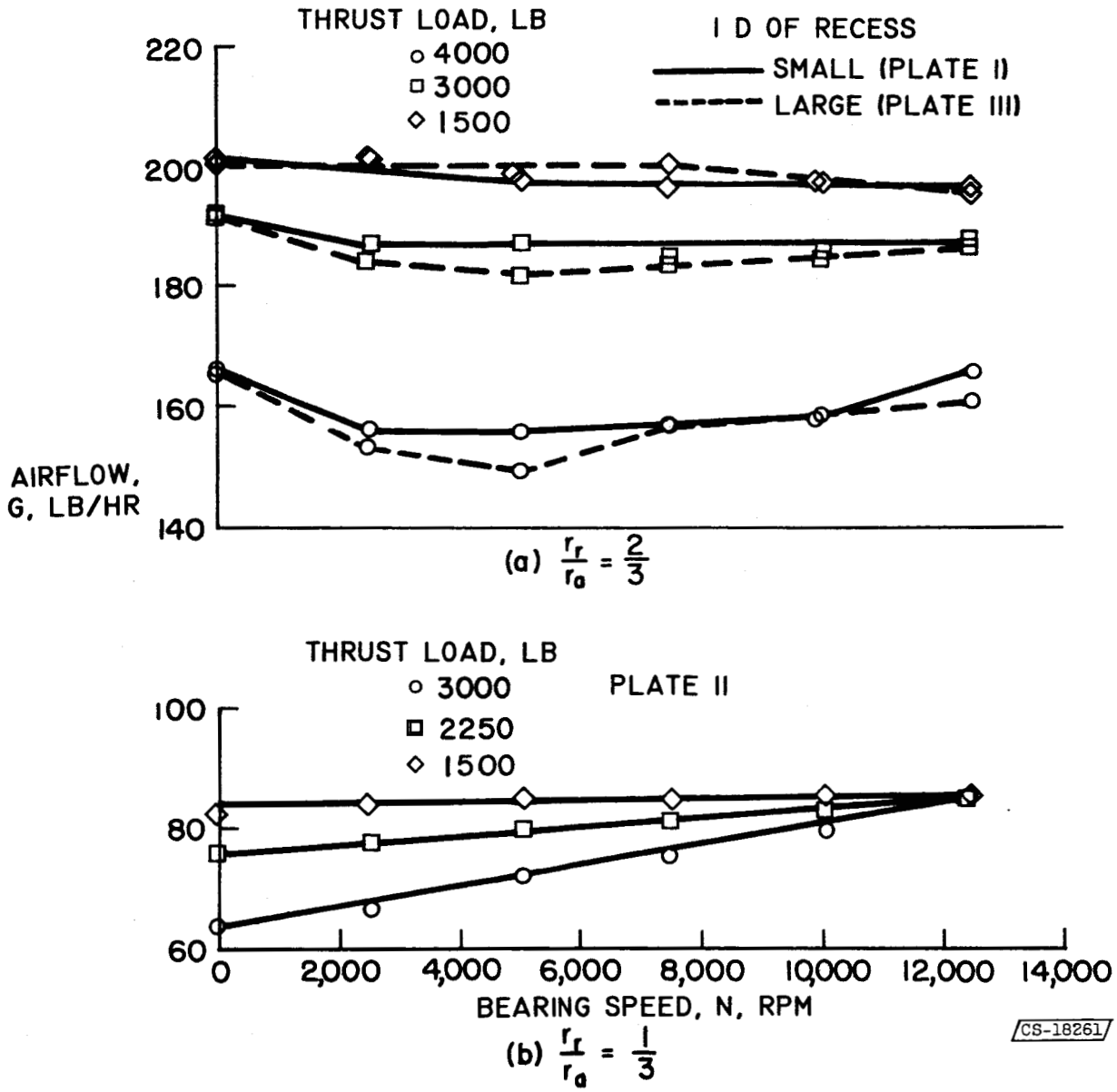

Fig. 5. - Effect of speed on bearing airflow. p_m = 114.7 psia.

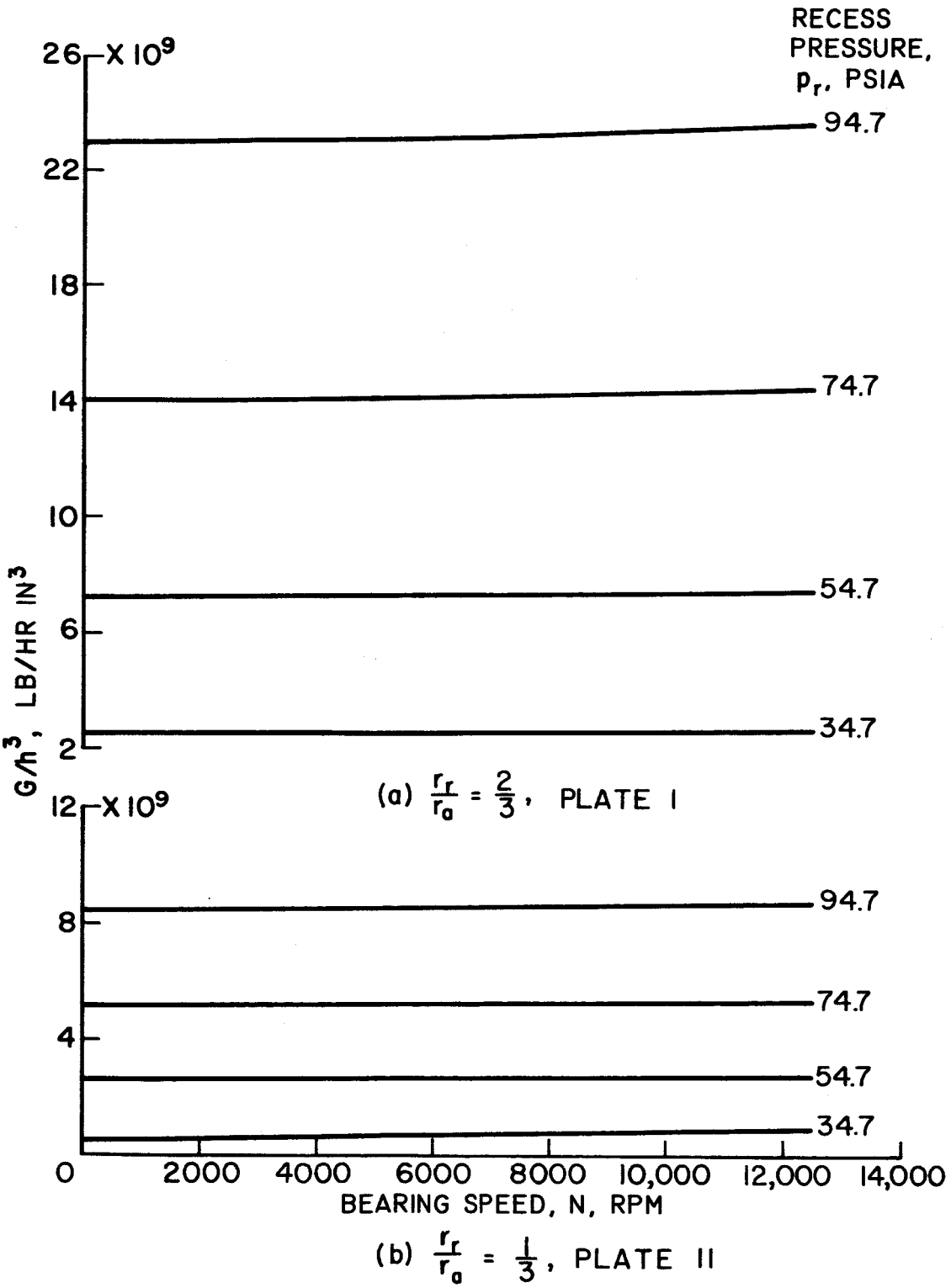

Fig. 6. - Theoretical effect of speed on G/h^3 for the simple bearing configuration of figure 2(d).

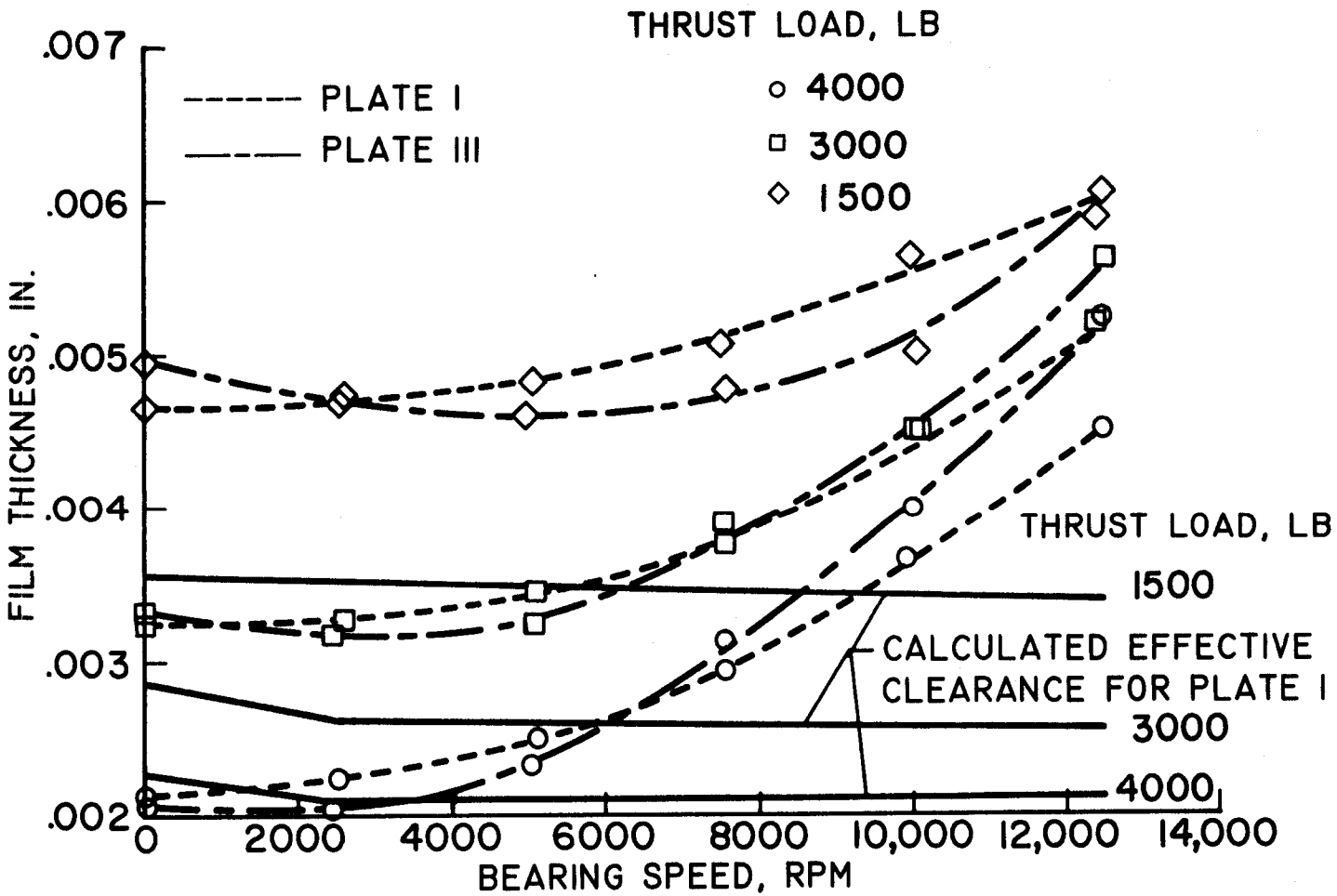

Fig. 7. - Effect of speed on measured film thickness 1.19 inches from the bearing axis and on calculated effective film thickness controlling bearing airflow. $r_r/r_a = 2/3$; $p_m = 114.7$ psia.

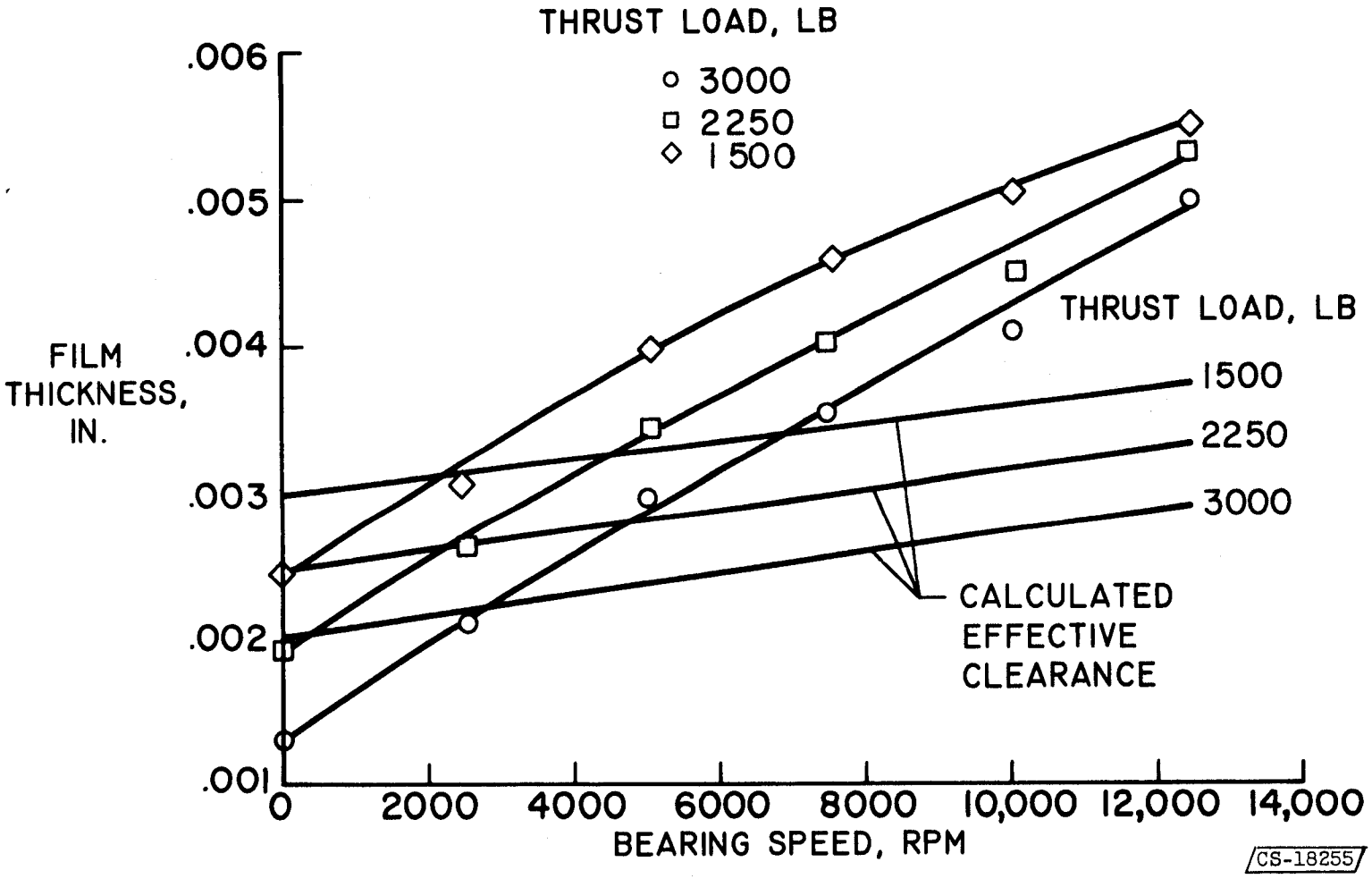

Fig. 8. - Effect of speed on measured film thickness 1.19 inches from the bearing axis and on calculated effective film thickness controlling bearing airflow. r_r/r_a = 1/3, Plate II; p_m = 114.7 psia.

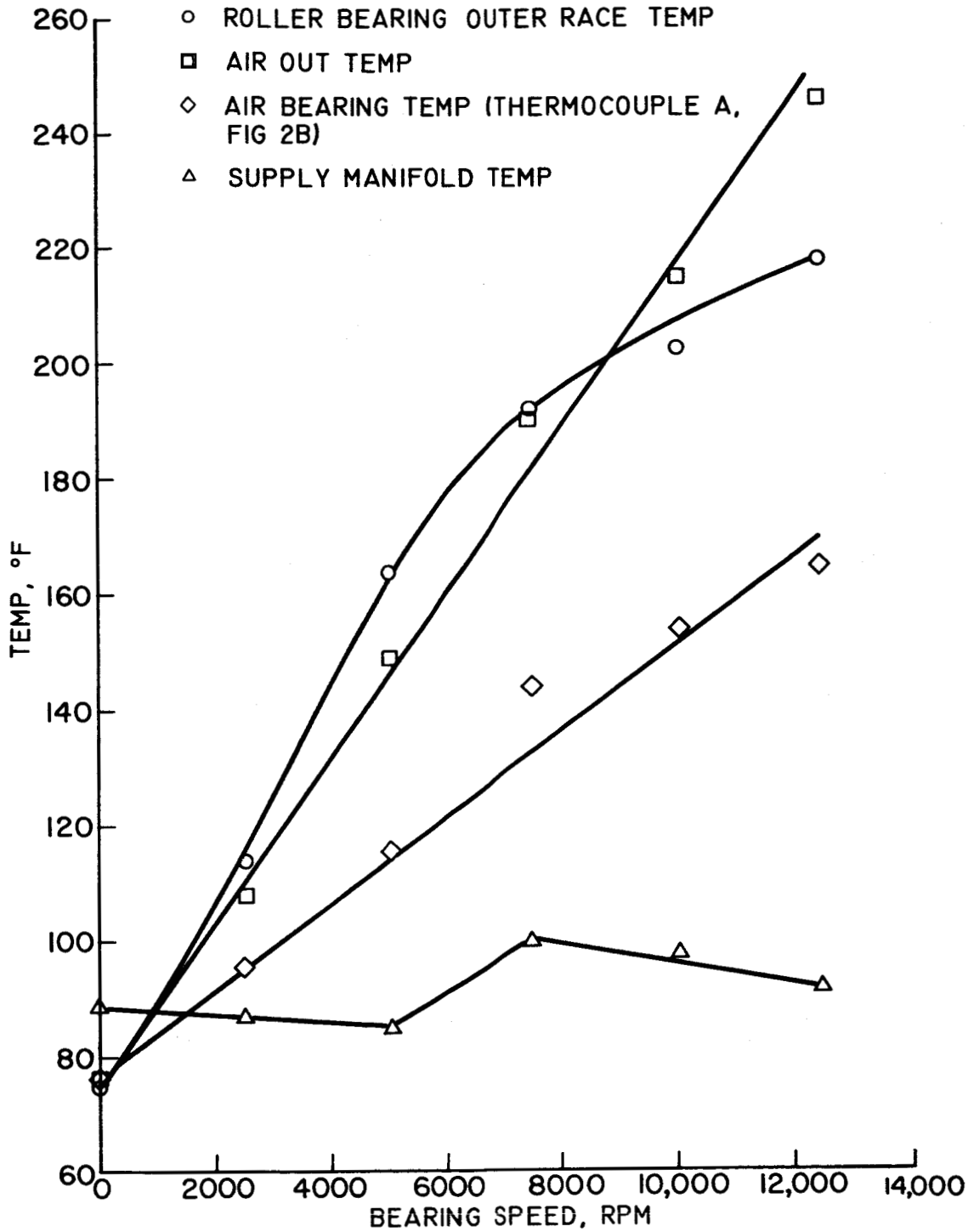

Fig. 9. - Temperatures as functions of speed for Plate II (r_r/r_a = 1/3). Load, 3000 pounds; p_m = 114.7 psia.

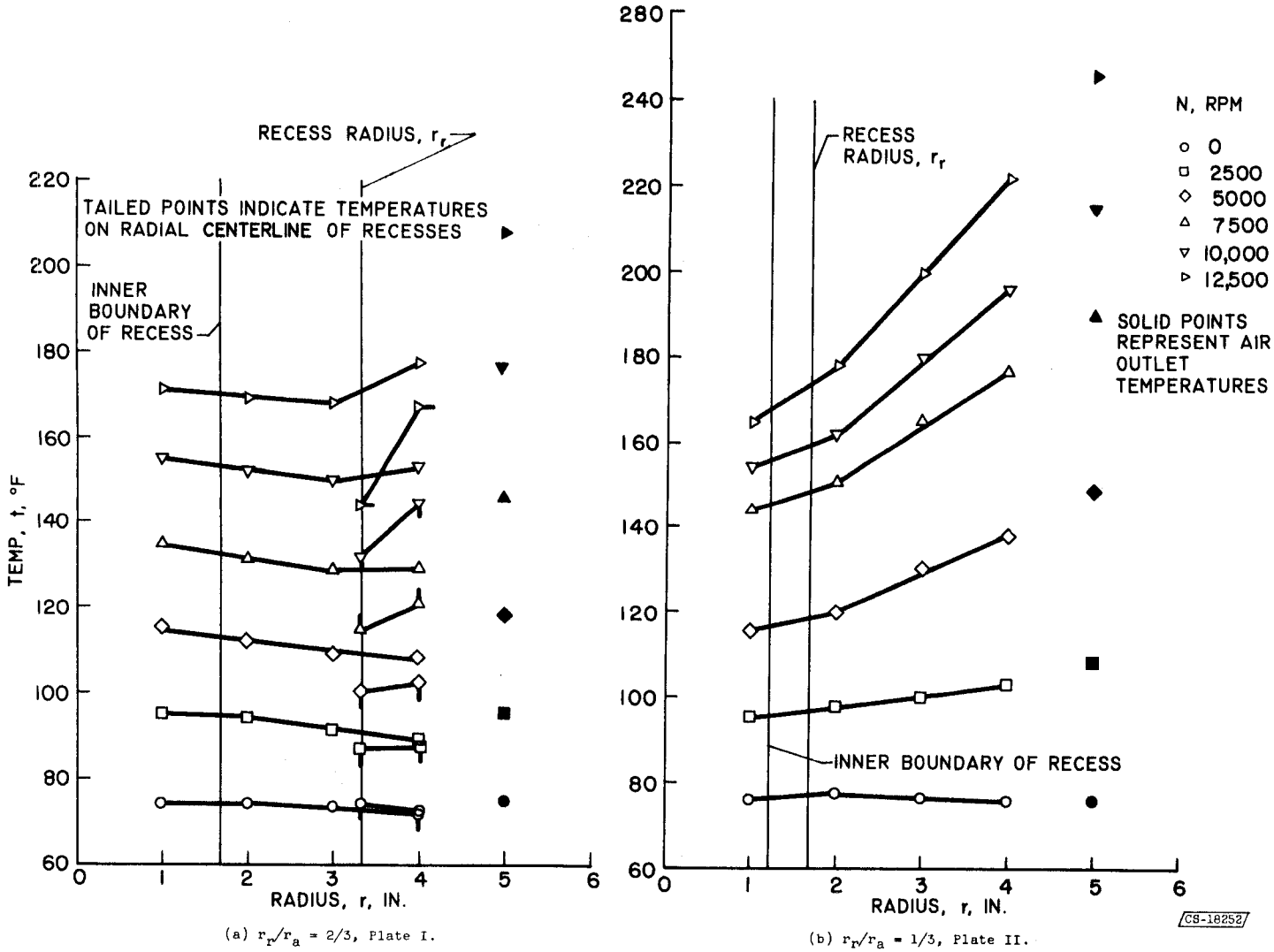

(a) r_r/r_a = 2/3, Plate I.

(b) r_r/r_a = 1/3, Plate II.

Fig. 10. - Bearing temperature profiles at various speeds.

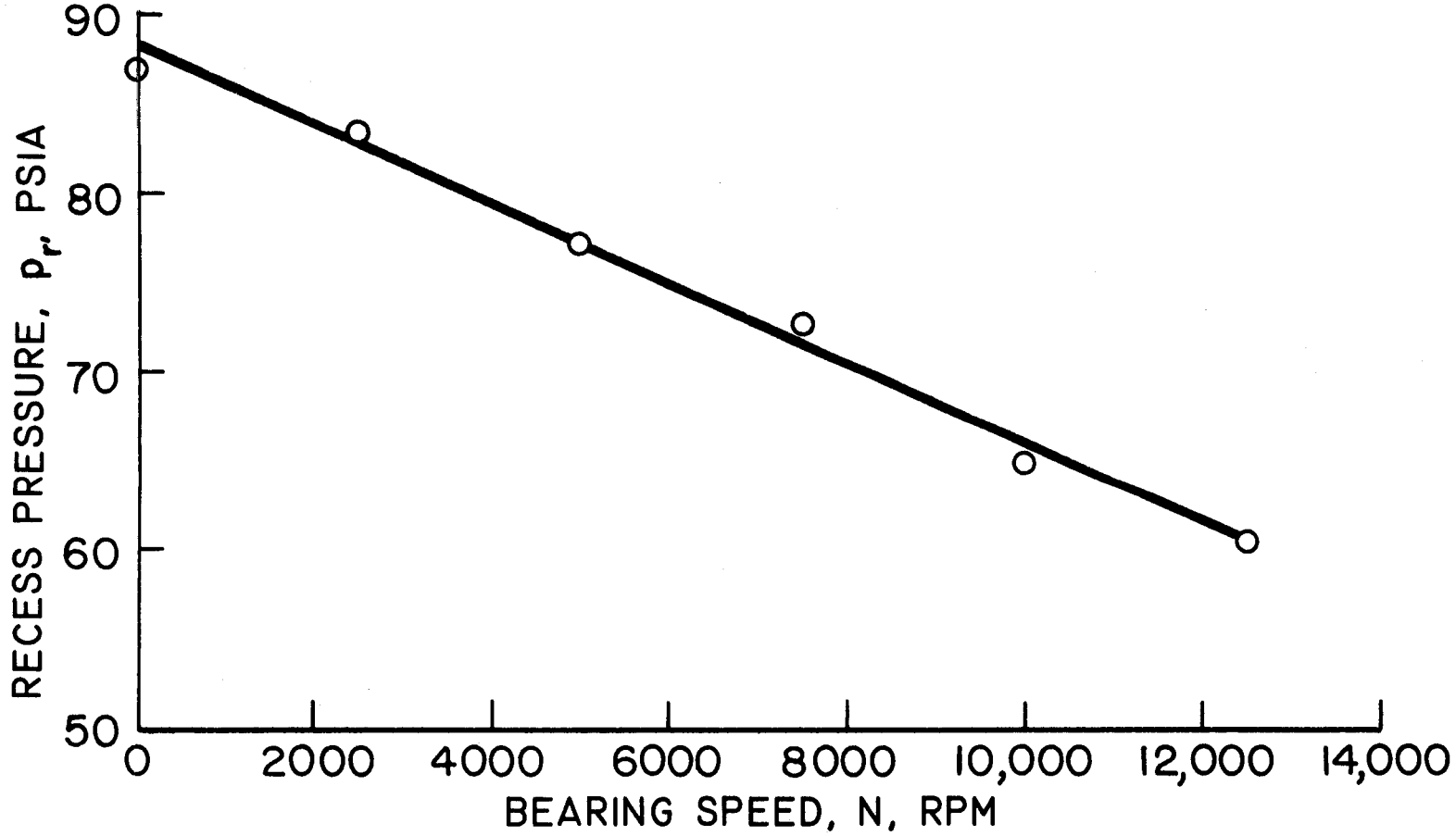

Fig. 11. - Effect of bearing speed on the recess pressure resulting with 3000 pounds load. $r_r/r_a = 1/3$, Plate II; $p_m = 114.7$ psia.

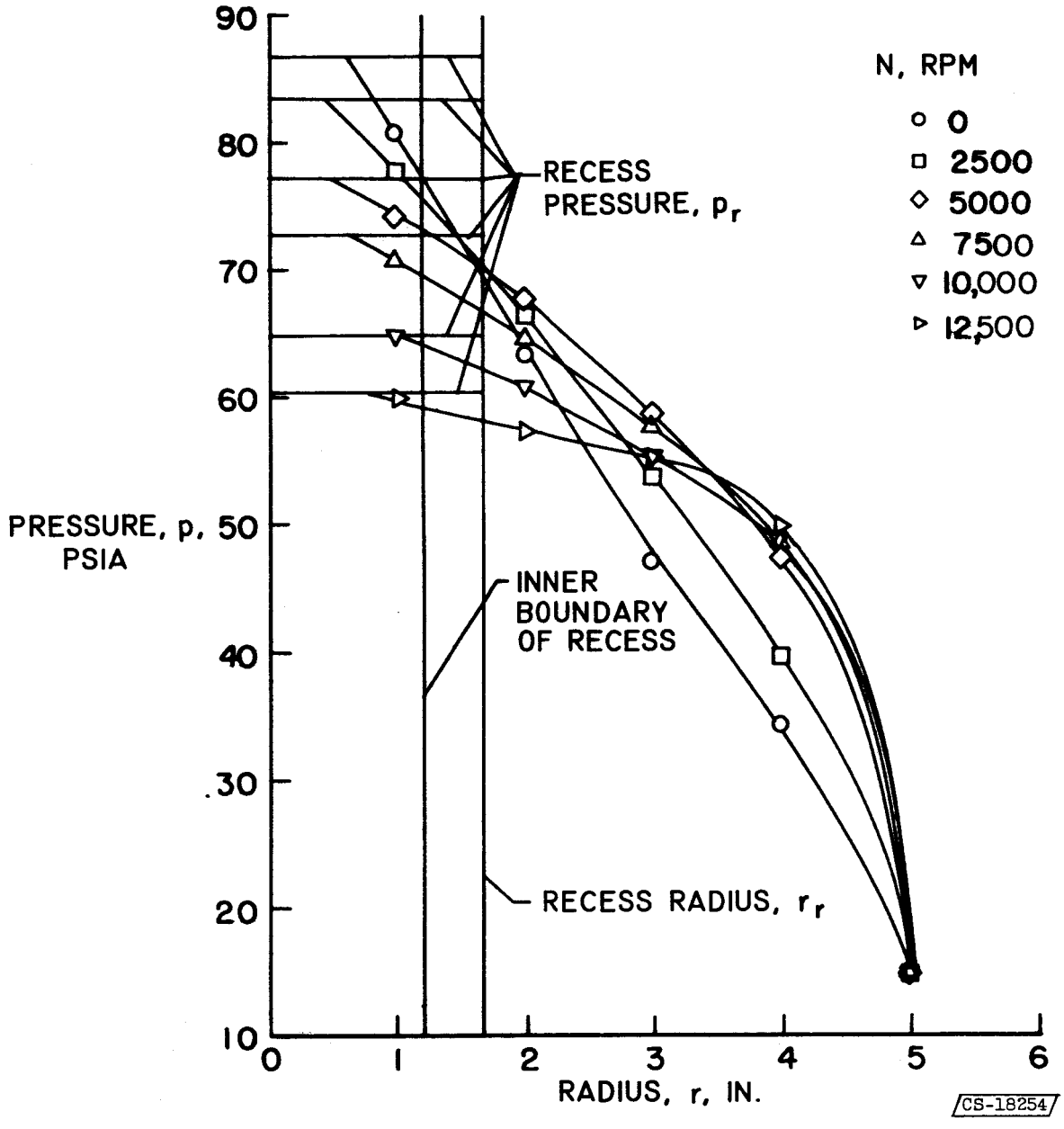

Fig. 12. - Pressure profile as a function of bearing speed. r_r/r_a = 1/3, Plate II; p_m = 114.7 psia; W = 3000 pounds. Pressures measured on the bearing land between recesses.

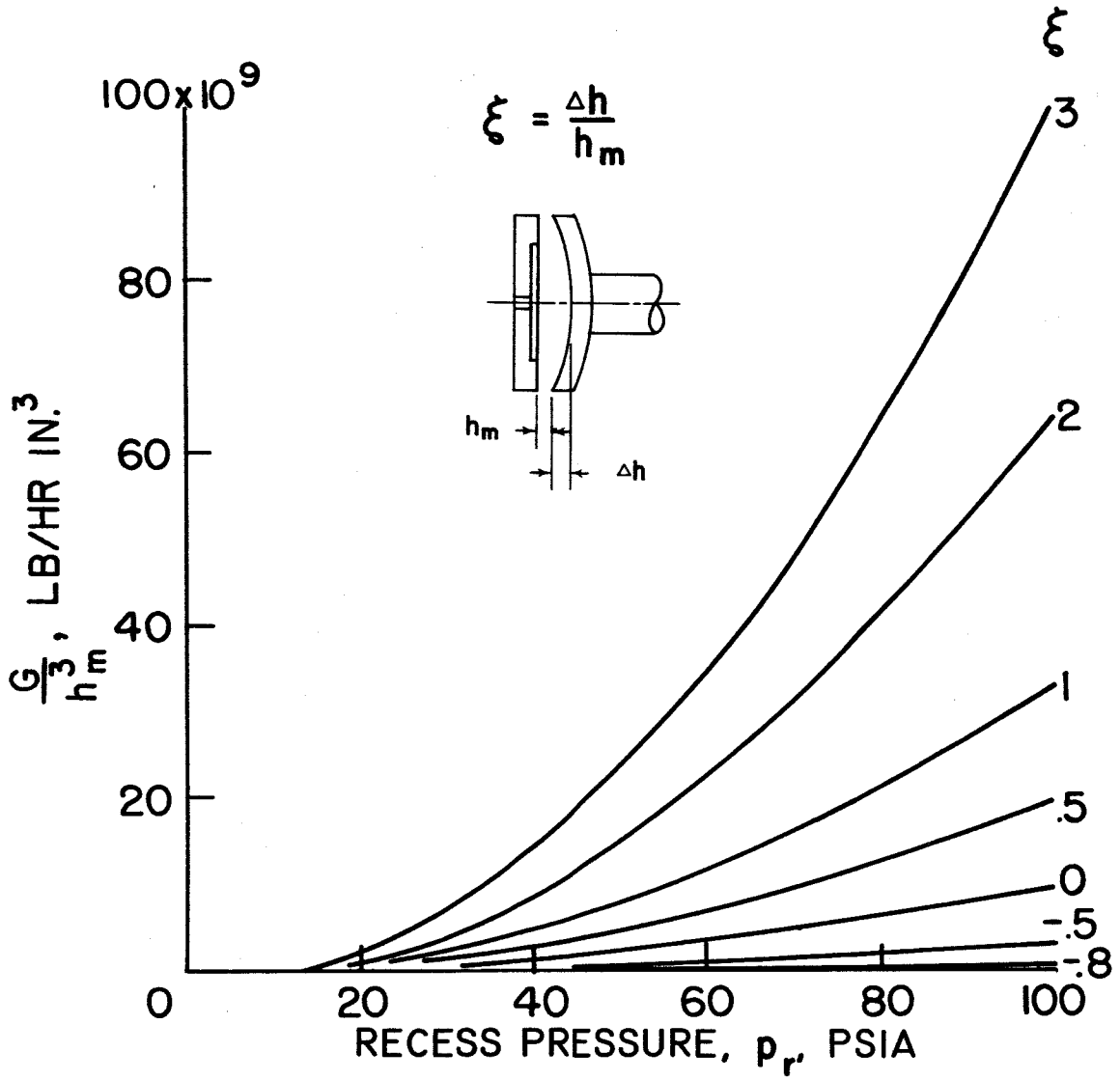

Fig. 13. - Theoretical effect of plate dishing on bearing airflow. $r_r/r_a = 1/3$.

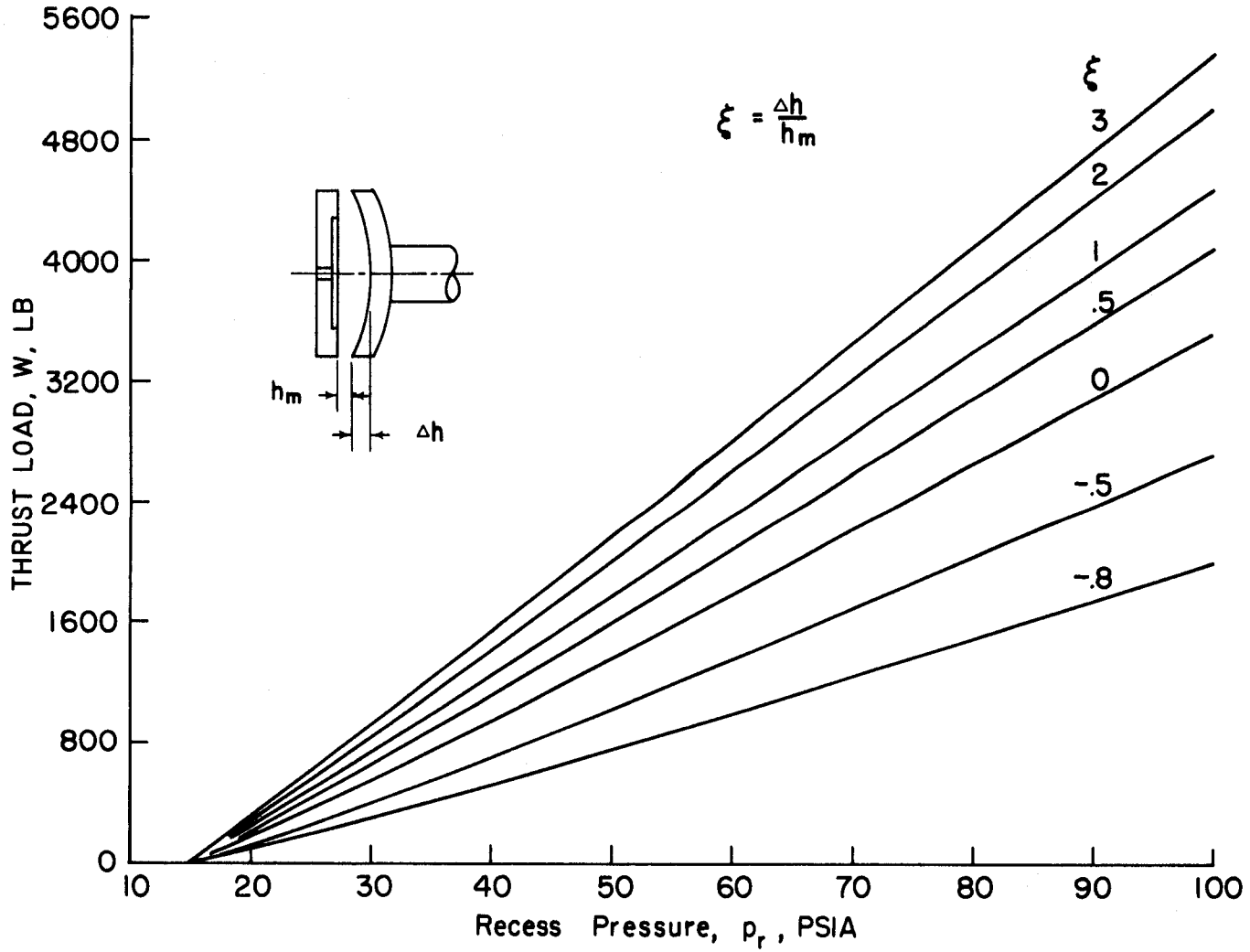

Fig. 14. - Theoretical effect of plate dishing on bearing load capacity. $r_r/r_a = 1/3$.

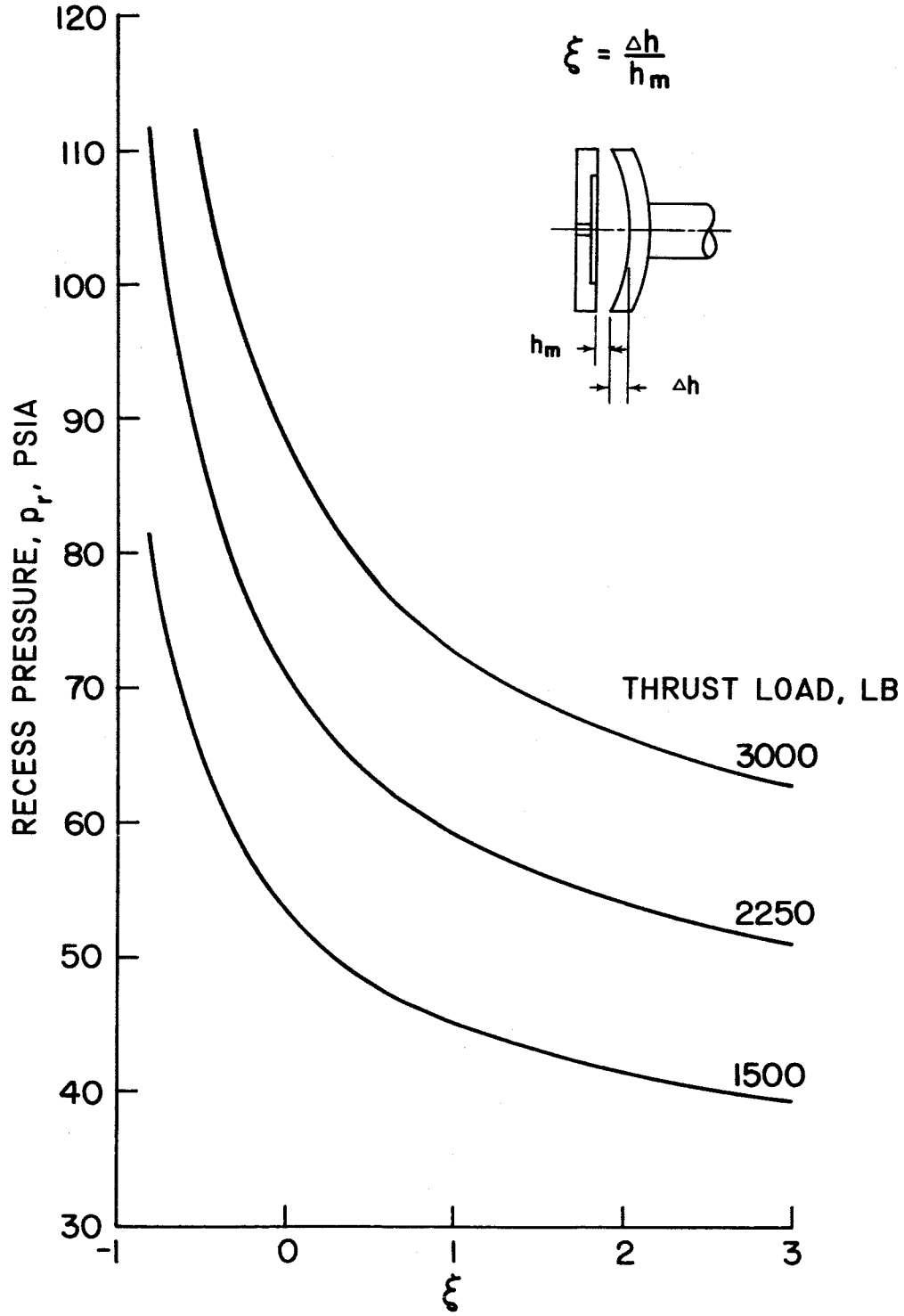

Fig. 15. - Theoretical bearing recess pressure required to support a given load as a function of the degree of dishing. $r_r/r_a = 1/3$.

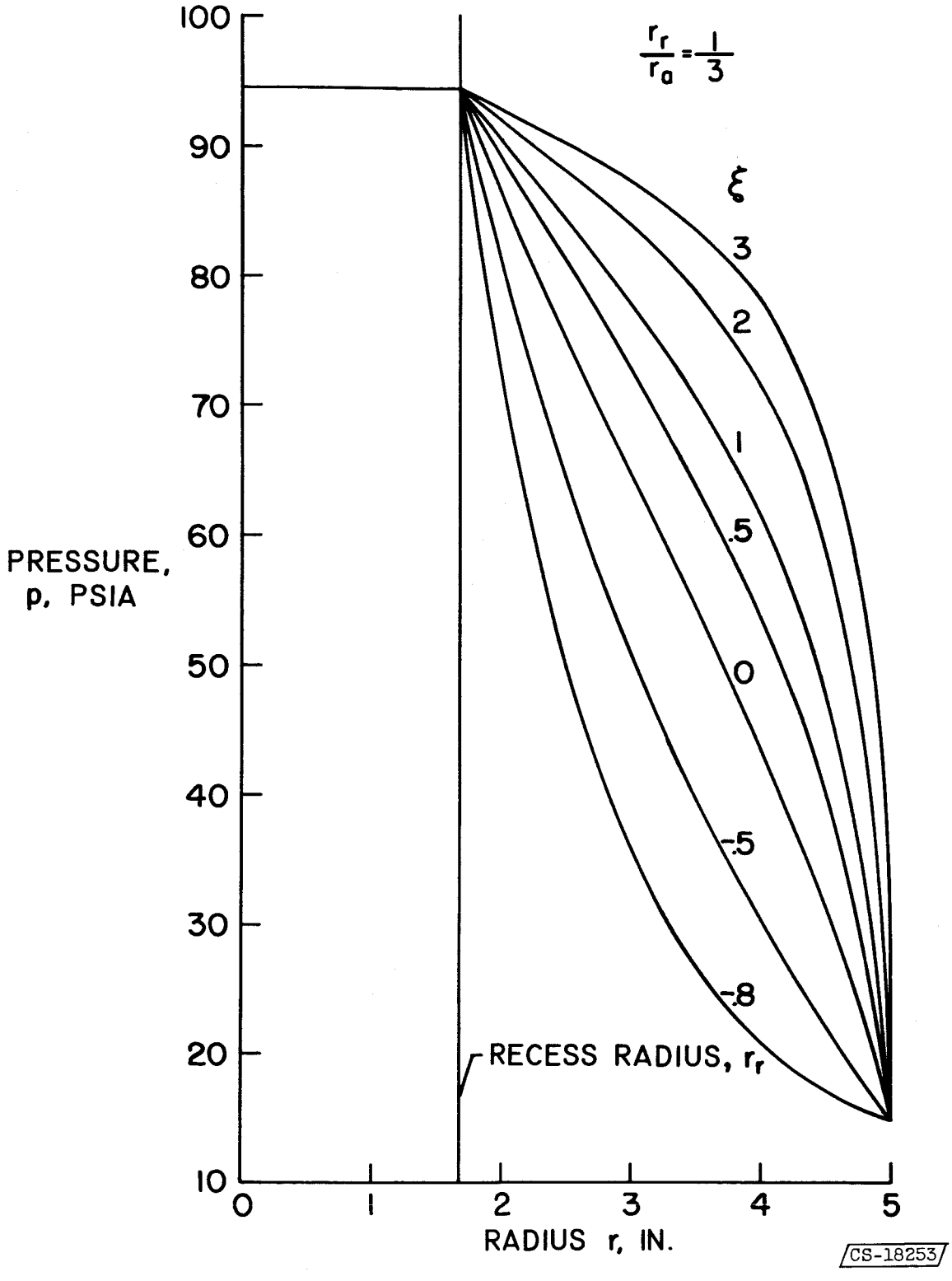

Fig. 16. - Theoretical pressure profile as a function of the degree of dishing $r_r/r_a = 1/3$; $p_r = 94.7$ psia.

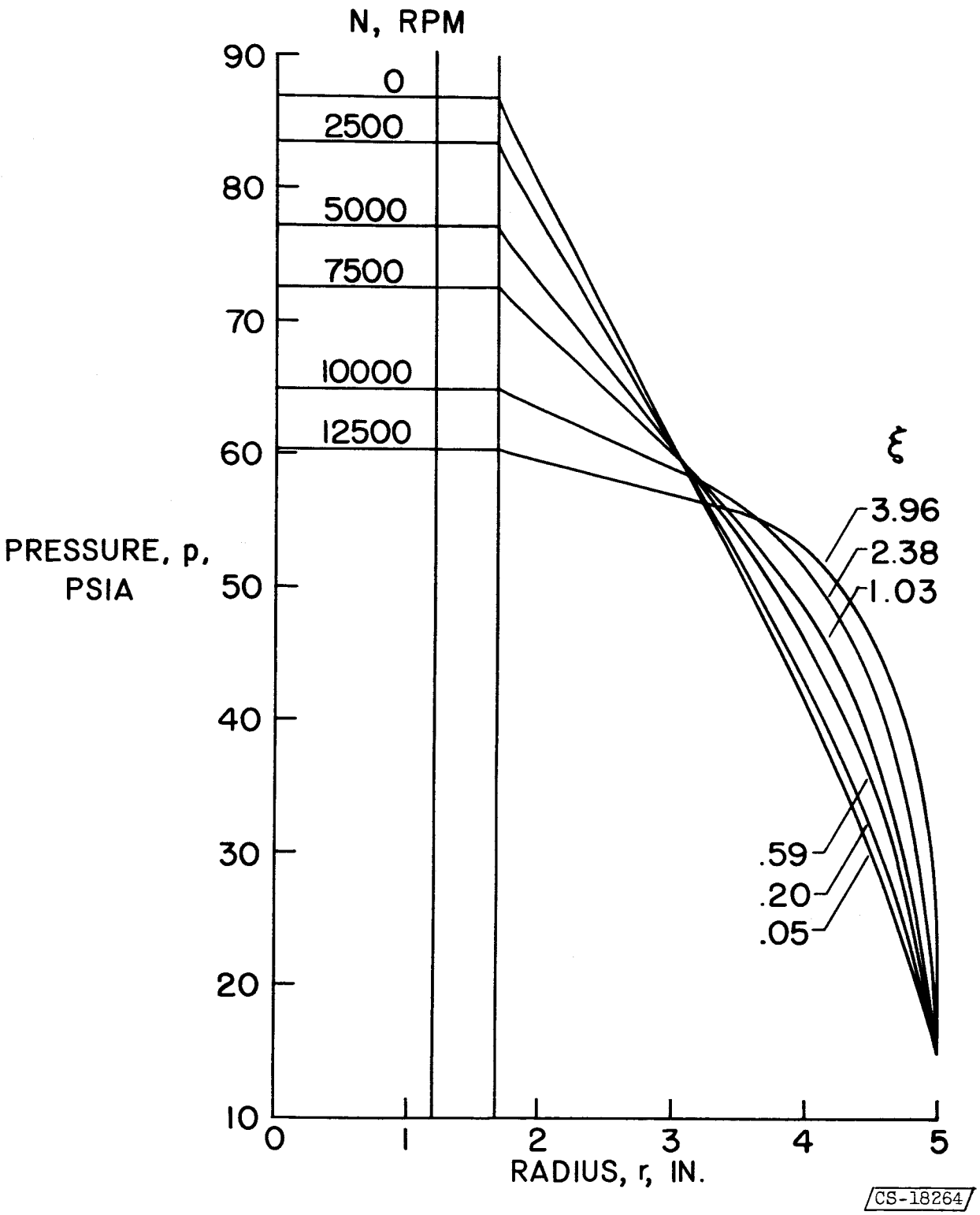

Fig. 17. - Theoretical pressure profiles at various speeds at 3000 pounds load. $r_r/r_a = 1/3$.